Downloaded from https://www.lyellcollection.org by University of Liverpool on Jan 26, 2023

Porosity in mudstones and its effectiveness for sealing carbon capture and storage sites

Nourah AlNajdi and Richard H. Worden*

Department of Earth, Ocean and Ecological Sciences, School of Environmental Sciences, University of Liverpool, Liverpool L69 3GP, UK

RHW, 0000-0002-4686-9428

*Correspondence: RHW, r.worden@liverpool.ac.uk; NA, n.alnajdi@liverpool.ac.uk

Abstract: Mudstones represent top-seals for many carbon capture sites as they tend to have the correct petrophysical properties, including suitable porosity and pore-size distribution. The pore network of mudstones is thus pivotal for many carbon capture and storage (CCS) projects. The key to understanding the effectiveness of top-seals is an appreciation of the controls on the pore network. For this reason, schemes to classify pore body size, pore type and pore throat size are presented. Pore types include primary and secondary interparticle and intraparticle pores and pores associated with organic matter and fractures. The most relevant mudstone pore body sizes for CCS top seals are likely to be between <62 µm and 1 nm. Pore throat sizes are classified as nano- (<10 nm), transition- (10 nm–0.1 µm), meso- (0.1–0.625 µm), and macro-pore throats (>0.625 µm). Petrophysical, geochemical, and geomechanical properties control porosity and the CO_2 sealing integrity of mudstones; these properties are, in turn, controlled by the rate and extent of compaction, mineral diagenesis and overpressure. The success of a CCS top-seal relies on pore throats in intact top-seal being sufficiently small, and fracture pressure (typically minimum horizontal stress, σ_{hmin}) not being exceeded by CO_2 pressure. CO_2 sorption, especially by smectite in top-seals, may improve the nanoscale sealing efficiency of clay minerals. The systematic workflow presented here will help facilitate the new drive to understand mudstone properties, as they are essential for establishing safe and durable CO_2 containment.

Mudstones commonly occur as top-seals for natural hydrocarbon accumulations, which makes them suitable candidates for sealing CO_2 during Carbon Capture and Storage (CCS) projects (Ingram and Urai 1999; Loucks *et al.* 2009, 2012; Aplin and Macquaker 2011; Kaldi *et al.* 2011; Espinoza and Santamarina 2012; Armitage *et al.* 2013; Busch and Amann-Hildenbrand 2013; Worden *et al.* 2020).

Pores in mudstones have a significant role in controlling mudstones' performance as top-seals; plus shale gas and shale oil production rates are strongly influenced by porosity and pore sizes (Slatt and O'Brien 2011; Curtis *et al.* 2012; Loucks *et al.* 2012; Busch *et al.* 2017). The porosity of mudstones has been reported to control the leakage risk of injected CO_2 from CCS sites (Busch *et al.* 2008, 2017; Busch and Amann-Hildenbrand 2013; Worden *et al.* 2020). Porosity also influences the rate of mineral reactions in mudstones, which then affects their geomechanical and petrophysical properties (Kampman *et al.* 2016; Busch *et al.* 2017).

Assessment of porosity in mudstone is complicated for several reasons. Mudstones have not typically been cored during the exploration, appraisal and development of conventional petroleum reservoirs, resulting in a relatively small archive of top-seal cores in comparison to reservoir cores in otherwise data-rich, mature, petroleum-producing regions (Alcalde *et al.* 2019). Work on shale as unconventional reservoirs is typically carried out on cuttings samples (Busch and Amann-Hildenbrand 2013; Busch *et al.* 2017), despite the commercial investment in shale gas (Slatt and O'Brien 2011; Loucks *et al.* 2012; Busch *et al.* 2017). Mudstone cores, when they have been collected, are not always stored in ways to avoid the effects of drying-out, swelling of smectite-rich layers, and oxidation of redox sensitive minerals, collectively leading to loss of sedimentary structures, mineral alteration or mechanical disintegration (Ewy 2015; Busch *et al.* 2017). All of these processes can cause difficulties in sample preparation and minimize the chance of quantifying, or studying, mudstone pore networks (Busch *et al.* 2017).

Flow networks in mudstone are formed by the connection of matrix-related pores via nanometre to micrometre pore throats, which, with the addition of fractures, act as conduits that control permeability and create pathways for fluid flow (Loucks *et al.* 2012). Different types of pores have been identified in fine-grained sediments, such as shales and mudstones (Desbois *et al.* 2009; Loucks *et al.* 2009, 2012; Passey *et al.* 2010; Lu *et al.* 2011; Slatt and O'Brien 2011; Curtis *et al.* 2012; Dernaika *et al.*

From: Miocic, J. M., Heinemann, N., Edlmann, K., Alcalde, J. and Schultz, R. A. (eds) *Enabling Secure Subsurface Storage in Future Energy Systems*. Geological Society, London, Special Publications, **528**,
https://doi.org/10.1144/SP528-2022-84
© 2023 The Author(s). This is an Open Access article distributed under the terms of the Creative Commons Attribution License (http://creativecommons.org/licenses/by/4.0/). Published by The Geological Society of London.
Publishing disclaimer: www.geolsoc.org.uk/pub_ethics

Downloaded from https://www.lyellcollection.org by University of Liverpool on Jan 26, 2023

2017; Wang *et al.* 2019). The term mudrock has been previously used to include both shale and mudstone (Ingram and Urai 1999; Loucks *et al.* 2012; Busch and Amann-Hildenbrand 2013; Busch *et al.* 2017; Peng *et al.* 2017; Zhang *et al.* 2018). Here, we will employ the collective term 'mudstone' as it is generic, it does not refer to the development of fissility (Aplin and Macquaker 2011) and the term mudstone forms a natural continuum with the terms siltstone and sandstone.

This paper presents a background to mudstone top-seals for CCS sites. It emphasizes the different classification schemes for pore body sizes and pore throat sizes in mudstone and what is relevant for CCS top seals, focusing on aspects that effect the pore network. The paper shows how mudstone porosity varies with depth and details the controls on mudstone porosity at various stages of burial. Finally, the paper addresses CCS top-seal leakage risks. To address these issues, the following research questions are addressed.

(1) What makes an effective seal?
(2) Does a given mudstone make a good seal to a CO_2 storage site?
(3) What are the origins of pores in mudstones?
(4) What controls the porosity of mudstones?
(5) What are the effects of CO_2 on mudstone top seal?

Does a mudstone seal?

In comparison to the amount of research and technical studies undertaken on sandstones and carbonates, mudstones initially experienced relatively little attention, however there has been increasing study of the mineralogy and texture of mudstones since shale gas became a commercial reality (Aplin and Macquaker 2011). The importance of mudstones has now been appreciated in conventional petroleum exploration and production, shale gas production, and in carbon capture and storage projects (Aplin and Macquaker 2011; Loucks *et al.* 2012; Armitage *et al.* 2013; Worden *et al.* 2020). The distinctive petrophysical characteristics of mudstones (typically low permeability but variable porosity, and high capillary entry pressure) allows them to act not only as a top-seal but also as a flow barrier or baffle in conventional and unconventional reservoirs (Dewhurst *et al.* 2002; Aplin and Macquaker 2011; Espinoza and Santamarina 2012; Worden *et al.* 2020).

Injectivity, storage capacity, and containment of CO_2 are controlled by the petrophysical, geomechanical and geological properties of the storage formations (Ajayi *et al.* 2019; Ringrose 2020). When supercritical or gas phase CO_2 is injected into the target formations designed for CCS, it must be trapped securely on a timescale of tens of thousands to millions of years, through a combination of structural and stratigraphic trapping as well as residual trapping and solubility trapping (Fig. 1) (IPCC 2005; Ajayi *et al.* 2019; Ringrose 2020). Mineral trapping will probably not play a major role in the containment of CO_2 on a human timescale in most sedimentary CCS sites as the supply of cations to lock away CO_2 as carbonate minerals and the kinetics of mineral growth are not favourable (Hellevang *et al.* 2013).

What makes an effective seal?

Evaluation of top seals is a critical step toward long-term secure CO_2 storage in the subsurface (Lohr and Hackley 2018). Geological storage of CO_2 ideally requires a low permeability seal with no post-injection alteration to the integrity of the storage site (Busch *et al.* 2010). The routine occurrence of highly pressured natural gas reservoirs with mudstone top-seals suggests that mudstones are likely to be effective for containing and preventing leakage of CO_2 (Busch *et al.* 2010).

Seal potential is a function of seal capacity, seal geometry and seal integrity. Seal capacity, defined by capillary entry pressure, controls CO_2 column height (Kaldi *et al.* 2013; Lohr and Hackley 2018). Seal integrity includes geomechanical rock properties, and seal geometry includes the thickness, structural position, and the areal extent of mudstone (Kaldi *et al.* 2013; Lohr and Hackley 2018).

Seal capacity

Seal capacity plays a crucial part in determining the effectiveness of a top seal's ability to contain CO_2 (Lohr and Hackley 2018). Seal capacity in depleted fields can be determined via empirical observations of the original hydrocarbon column height and converting to CO_2 column height by accounting for the physical properties of CO_2 compared to the original hydrocarbon (Divko *et al.* 2010; Kaldi *et al.* 2013; Lohr and Hackley 2018). Pore throat size, interfacial tension (IFT), and contact angle (wettability) are the dominant controls on the seal capacity (CO_2 column height) of a mudstone (Lohr and Hackley 2018).

Mercury injection capillary pressure (MICP) on small pieces of mudstone top-seal can be used to determine seal capacity and maximum CO_2 column height (Kaldi *et al.* 2013; Lohr and Hackley 2018; Worden *et al.* 2020). For example, the likelihood of CO_2 leakage from the potential Acorn and East Mey CCS sites was determined using MICP. The maximum CO_2 column heights for 16 top seals samples were determined from the Lower Cretaceous

Downloaded from https://www.lyellcollection.org by University of Liverpool on Jan 26, 2023

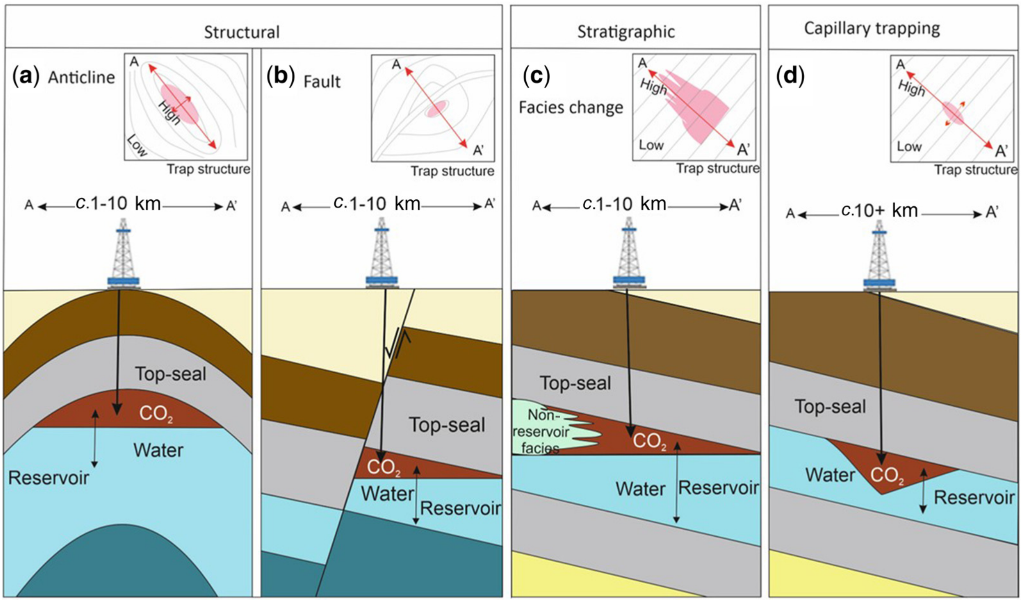

Fig. 1. Schematic diagram of the different kind of physical trapping mechanisms of CO_2 associated with the structure and geometry of the trap. The injectivity, storage capacity and containment of CO_2 are reliant on geological properties of the storage formations. At temperatures and pressures typically found >800 m, CO_2 occurs as a supercritical fluid (Span and Wagner 1996; Espinoza and Santamarina 2017; Ajayi *et al.* 2019; Ringrose 2020). The density of supercritical CO_2 is lower than water, so that CO_2 buoyantly rises above the saline formation water (Espinoza and Santamarina 2017; Ajayi *et al.* 2019; Ringrose 2020). Structural traps are formed by either folding or faulting whereas stratigraphic traps result from lateral (up-dip) change from reservoir to non-reservoir. (**a**) Anticlinal structural trap where CO_2 rises above the formation water below the overlying impermeable mudstone seal. (**b**) Fault structural trap which requires both a top-seal (here a mudstone) and either a fault-seal or juxtaposition of reservoir against a sealing lithology. (**c**) Stratigraphic traps created by lateral facies changes in the permeable formation, with an overlying top-seal (Tiab and Donaldson 2016*a*). (**d**) Injected CO_2 will rise up in a spreading plume with a shape controlled by a combination of viscosity and buoyancy (gravity) forces. Capillary trapping operates when pore throats are too small to allow non-wetting phase CO_2 to migrate or when the CO_2 saturation is too low (Krevor *et al.* 2015).

Rodby Shale from the Acorn CCS site and the Paleocene Lista shale from the East Mey CCS site (Worden *et al.* 2020). It was concluded that the risk of CO_2 leakage is low as the maximum CO_2 height column of both top seals is greater than the closure of the trapping structure of the petroleum system (Worden *et al.* 2020).

Seal geometry

The thickness and lateral extent of a caprock is referred to as seal geometry (Kaldi *et al.* 2013). A caprock must have sufficient lateral width and length to overlay the full extent of the greater trap that is required to contain CO_2 (Kaldi *et al.* 2013). Moreover, the caprock should be thick enough to maintain an effective seal against any faults (Kaldi *et al.* 2013). Evaluation of seal geometry can be conducted through wireline log data, seismic analysis, and detailed stratigraphic and sedimentological analysis (Kaldi *et al.* 2013).

Seal integrity

Seal integrity can be compromised by fracture networks, fault systems, and geochemical stability factors (Lohr and Hackley 2018). Faults and fractures have the ability to either improve or slow the rates of fluid migration (Kaldi *et al.* 2013). According to Kaldi *et al.* (2013), there are three important points to consider in order to define the influence of faults and fracture on CO_2 migration; (1) understand the properties of any faults and fractures in the targeted storage reservoir and top-seal in terms of their location, geometry, timing of development, extent of displacement and microstructure, and juxtaposition of different lithologies across a fault; (2) consider the impact of the faults and fractures on the flow of CO_2 during and after injection; (3) address how the behaviour of the faults and fractures will be affected by induced or natural stresses. It may be essential to understand the origin of microstructure associated with faults including cataclasis, cementation, grain sliding, and

Downloaded from https://www.lyellcollection.org by University of Liverpool on Jan 26, 2023

clay smear, which together determine whether the fault is a seal or conduit (Kaldi *et al.* 2013).

Capillary entry pressure

In general, when CO_2 fluid pressure in the reservoir exceeds the capillary entry pressure, migration of the CO_2 through the water-saturated porous network of a caprock may take place (Hildenbrand *et al.* 2004; Busch *et al.* 2010). Quantitative evaluation of an effective seal requires investigation of several transport processes and capillary pressure phenomena (Hildenbrand *et al.* 2004). Displacement pressure is the key parameter for characterizing capillary sealing efficiency; displacement pressure is defined as the minimum capillary entry pressure above which the seal tends to leak (Hildenbrand *et al.* 2004). Specifically, the capillary entry pressure of a caprock to a CCS site is controlled by the capillary forces of the rock matrix including pore throat radius, the CO_2–brine–mineral contact angle, and the CO_2–brine interfacial tension (Busch *et al.* 2010).

Genetic porosity classification and its origin in top seals

Pore body size classification schemes

The word pore in the context of CCS systems is potentially ambiguous as it refers to both pore throats and open pores. Here we adopt the term 'pore body' to reflect the maximum dimension across a pore. The term pore throat is used to represent the maximum dimension of the opening between grains that connects adjacent pore bodies (Yang and Aplin 1998).

Pore size classifications of mudstones have been reconsidered over the last 20 years, largely because the shale-gas industry has led to a new demand for high quality mudstone characterization. In general, pore size is defined as the maximum width of a pore (body), which is the distance between two opposite walls (Rouquerol *et al.* 1994). Although it is important to characterize pore sizes in porous media, it has proved to be a nebulous concept, dependent on the technique employed (Rouquerol *et al.* 1994).

A pore size classification scheme was proposed by Rouquerol *et al.* (1994), created from the International Union of Pure and Applied Chemistry (IUPAC) scheme for nanometre-scale pores. The IUPAC classification is based on the width of pores, regardless of their origin or pore shape. According to the Rouquerol *et al.* (1994) classification, micropores in mudstones smaller than 2 nm may have either a structural, intracrystalline origin, e.g. within minerals such as sepiolite, or a textural (intercrystalline) origin, e.g. between individual clay flakes. Mesopore widths in mudstones are between 2 and 50 nm and tend to have an intraparticle, and interparticle origin. Macropores in mudstones are larger than 50 nm, and they were reported to typically result from shielding against compaction by silt and sand grains (Rouquerol *et al.* 1994; Yven *et al.* 2007).

Loucks *et al.* (2012) suggested that, even though the Rouquerol *et al.* (1994) classification is suitable for chemical products such as membranes, it may not be suitable for fine-grained rocks such as shale reservoirs. Instead, the Choquette and Pray (1970) scheme, designed for carbonate pore classifications, was adapted by Loucks *et al.* (2012) for shale pore classification. The Choquette and Pray classification defines micropores (<62.5 µm), mesopores (62.5 µm to 4 mm), and megapores (4 to 256 mm). To deal with smaller classes of pores, Loucks *et al.* (2012) proposed two more subdivisions; nanopores (<1 µm) and picopores (<1 nm) (Fig. 2; Table 1).

Justification for CCS top-seal pore body size classification

Based on a classification scheme from unconventional shale reservoirs, mudstone pores (i.e. pore bodies) potentially vary in size from nanometres to micrometre in diameter (Loucks *et al.* 2012). For a top-seal to be effective, the porosity must be relatively low, and the pore bodies need to be small; as a consequence, it is highly unlikely that there will be pores >4 mm, or even pores between 62.5 µm and 4 mm. The micropores (1 to 62.5 µm) and nanopores (<1 µm) adopted from the (Loucks *et al.* 2012) are the types that are most likely to be relevant to CCS top seals. Therefore, the pore body sizes in CCS top seals fall the range between (<62 µm–1 nm). The picopore subdivision, important for the desorption of gas in shale reservoirs (Wang *et al.* 2019), is probably relatively unimportant for CCS topseals (Fig. 2; Table 1).

Definition of pore types

By definition, mudstones are initially dominated by detrital materials that are smaller than 62.5 µm (Loucks *et al.* 2012). Mudstones typically remain fine-grained even after going through physical and chemical processes during burial and mineral diagenesis (Aplin and Macquaker 2011; Loucks *et al.* 2012). In soil science, particle size distribution is considered to be an essential parameter because it assists in defining fluid movement, pore body size distributions and air–water relationships (Polakowski *et al.* 2021). However, particle size is not the only factor that controls pore body size classes or mudstone attributes; other factors such as where the pore is, its origin, sorting, surface area, and capillary entry pressure also need to be considered. In the next section, we explore the origin and attributes of different types of pores in mudstones.

Downloaded from https://www.lyellcollection.org by University of Liverpool on Jan 26, 2023

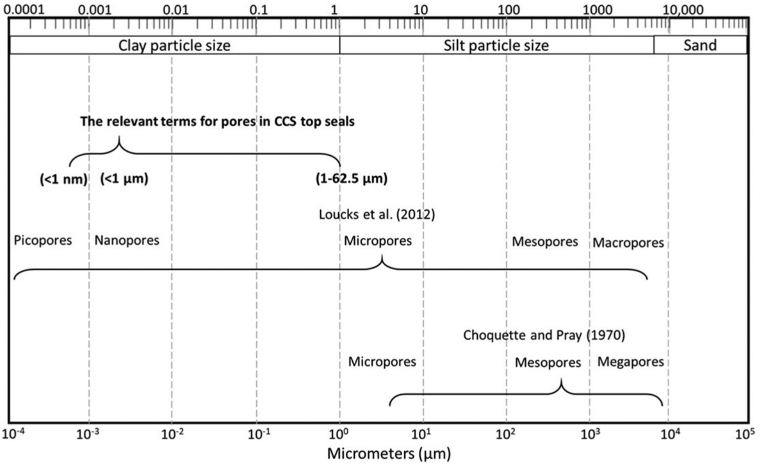

Fig. 2. Genetic pore body size classification schemes for fine-grained clastic and carbonate rocks. The lower axis is a log scale based on pore size values in micrometres (µm). The most common terms used in pore size classification literature are macropores, mesopores, micropores, nanopores and picopores. The terms relevant for pores in CCS top seals include micropores and nanopores with picopores probably not being very important.

Interparticle pores

Interparticle pores are pores between grains (Desbois *et al.* 2009; Loucks *et al.* 2009, 2012). Interparticle pores occur between clay minerals (clay platelets) and silt-grade material (Kwon *et al.* 2004; Loucks *et al.* 2012) (Figs 3 & 4a, b; Table 2). In many cases, interparticle pores are relatively well connected and typically contribute to permeability (Loucks *et al.* 2012). As overburden (vertical effective) stress increases and mechanical compaction (strain) and chemical diagenesis proceed, the interparticle pore network evolves (typically decreases) with time and increasing temperature (Loucks *et al.* 2012) (Fig. 3).

Table 1. *Summary of the definitions of pore body sizes in mudstone*

Origin	Divisions		Ranges	
Rouquerol *et al.* (1994)	(1)	Micropores	(1)	<2 nm
	(2)	Mesopores	(2)	2–50 nm
	(3)	Macropores	(3)	>50 nm
Choquette and Pray (1970)	(1)	Micropores	(1)	<62.5 µm
	(2)	Mesopores	(2)	62.5 µm to 4 mm
	(3)	Megapores	(3)	4–256 mm
Loucks *et al.* (2012)	(1)	Picopores	(1)	<1 nm
	(2)	Nanopores	(2)	<1 µm
	(3)	Micropores	(3)	1–62.5 µm
	(4)	Mesopores	(4)	62.5 µm to 4 mm
	(5)	Macropores	(5)	>4 mm

Intraparticle pores

Intraparticle pores exist within grains. Most intraparticle pores are diagenetic in origin, but some, such as intrinsic pores in bioclasts, are primary (Slatt and O'Brien 2011; Loucks *et al.* 2012) (Fig. 3). Intraparticle pores include moldic pores created by complete or partial dissolution (Fig. 4e, f), pores within fossils, such as foraminifera (Fig. 4g, h), or pores within pyrite framboids (Fig. 4i, j) (Loucks *et al.* 2009, 2012; Slatt and O'Brien 2011). The variation of pore size in framboidal pyrite is dependent on the size of the overall framboids; for example, small framboids of 2 to 10 µm in size exhibit pore from 0.05 to 1 µm in size (Loucks *et al.* 2009) (Fig. 4i, j) (Table 2).

Organic matter pores

Pores in organic matter have been well documented in shale gas reservoirs as organic matter can be both the source and host for methane in such reservoirs (Loucks *et al.* 2009; Slatt and O'Brien 2011) (Fig. 3). Pores associated with organic matter are the result of burial and organic matter maturation (Jarvie *et al.* 2007; Slatt and O'Brien 2011). The diameter of pores associated with organic matter occur at the nanometre scale and tend to be isolated (Slatt and O'Brien 2011). The development of organic matter pores in shale is affected by organic matter maturation, clay mineral content, and total organic carbon (TOC) (Li *et al.* 2016). Organic matter type depends on the composition of organic matter, lithology of the host and depositional

Downloaded from https://www.lyellcollection.org by University of Liverpool on Jan 26, 2023

Table 2. *Classification summary of the main pore body types based on their origin, order and occurrence in top seals*

Pore type	Origin	Order	Occurrence	Other terminology	References
Interparticle	Mineral matrix	Primary	Pores between the grains	Intergranular	Loucks *et al.* (2009, 2012), Slatt and O'Brien (2011)
Clay platelets	Mineral matrix	Primary	Pores within clay aggregates	Intra-clay aggregate	Loucks *et al.* (2009, 2012), Slatt and O'Brien (2011)
Intraparticle	Mineral matrix	Primary/ Secondary	Pores within grains	Intragranular	Loucks *et al.* (2009, 2012), Slatt and O'Brien (2011)
Moldic pores	Mineral matrix	Secondary	Pores due to partial or complete dissolution of primary material	Secondary intragranular	Loucks *et al.* (2012), Slatt and O'Brien (2011)
Framboidal pores	Mineral matrix	Secondary	Intercrystallite pores within pyrite framboids	Intercrystallite	Loucks *et al.* (2009, 2012), Slatt and O'Brien (2011)
Organic pore	Organic matter	Secondary	Pores in planktonic algae in the liptinite maceral group, such as boghead algae		Cardott and Curtis (2018)
Parallel bedding fractures	Shear	Secondary	Pores that form when all the stresses in the three principal directions are compressive		Tiab and Donaldson (2016*b*)
Cross-bedding fractures	Tensional	Secondary	Pores that form when one of the principal stresses is tensile		Tiab and Donaldson (2016*b*)
Stylolite	Pressure solution, tectonic	Secondary	Pores that result from burial-related chemical compaction or elevated tectonic stress		Humphrey *et al.* (2019), Bruna *et al.* (2019) and Koehn *et al.* (2016)

The most common types of pores are interparticle and intraparticle and are linked to the mineral matrix. The type of organic pores is dependent on their occurrence, for example as listed, boghead algae is a type of planktonic algae and classified as sapropelic according to coal classification schemes. Fracture types are listed based on their origin either from tectonic activity or normal burial processes.

environment (Cardott and Curtis 2018). Macerals, the organic equivalent of minerals, include all solid organic matter, such as vitrinite, and the solid (bitumen) part of kerogen (Cardott and Curtis 2018). For example, boghead algae is a planktonic algae that belongs to the liptinite maceral group (Peppers and Harvey 1997; Cardott and Curtis 2018). Boghead algae occur in tropical and temperate zones around the world, especially freshwater lakes (Peppers and Harvey 1997); some types of decomposed algae contain porosity (Peppers and Harvey 1997) (Fig. 4k, l; Table 2). While shale gas reservoirs must be rich in organic matter, typically with a total organic content greater than 2% (Tissot *et al.* 1974; Ma *et al.* 2017), and therefore have an appreciable volume of organic matter pores, mudstone top-seals to CCS sites are relatively unlikely to be organic-rich and probably will have few pores in organic matter.

Fractures

Fractures may act as seals or conduits to fluid flow depending on the degree of shearing-related comminution and mineralization (Tiab and Donaldson 2016*b*) (Fig. 3). Shear fractures can occur parallel, or at an angle, to bedding and typically display evidence of movement parallel to the fracture plane; they form when all three principal stresses are compressive (Tiab and Donaldson 2016*b*) (Fig. 4m, n). In contrast, cross fractures, also known as tensional fracture, have evidence displacement perpendicular to the fracture plane. For tensional fractures to

Downloaded from https://www.lyellcollection.org by University of Liverpool on Jan 26, 2023

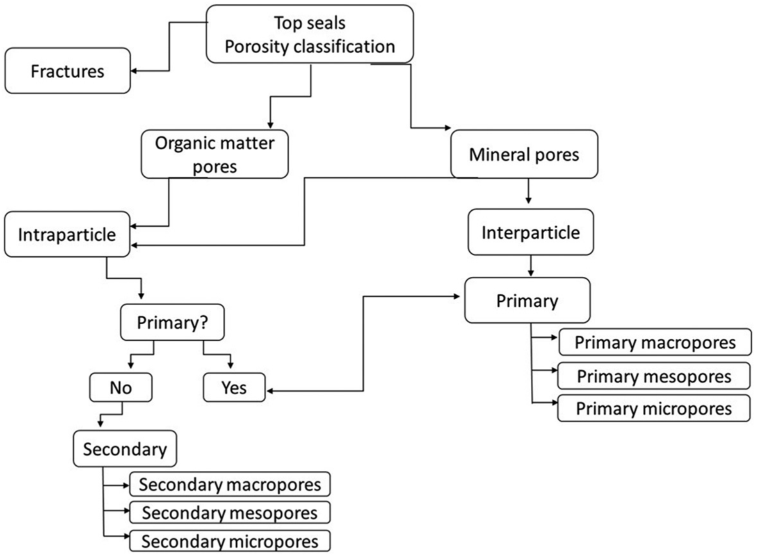

Fig. 3. A genetic classification scheme for determining the type of porosity found in top seals. The scheme links pore body sizes with pore types. The main pore types are mineral pores, organic matter pores, and fractures. When the porosity is interparticle and primary, then it leads to the classification of pore body sizes (Primary macropores, mesopores and micropores). If a given pore is classified as intraparticle, the investigation on the order of porosity start to take place. If the pore type is primary intraparticle, it falls back to the classification of primary pore body sizes. If not, then it will be classified as secondary porosity leading to the classification of pore body sizes (secondary macropores, mesopores and micropores). Secondary porosity is a result of diagenesis and dissolution of primary materials and early cements (Gluyas 2005).

occur, at least one of the principal stresses must be extensional (Tiab and Donaldson 2016*b*) (Fig. 4o, p) (Table 2). Cross fractures are more likely to be open and contribute to porosity than shear fractures but only if mineralization of the new fracture has not occurred.

Pores associated with stylolite

Stylolites are uneven surfaces that result from intergranular dissolution processes and are found in many rock types (Koehn *et al.* 2007, 2016; Bruna *et al.* 2019). There are two main types of stylolites: (i) bedding-parallel stylolites in otherwise undeformed rocks, in which bedding is still horizontal, where the vertical effective stress is equal to the maximum principal stress, and (ii) tectonic stylolites that form as result of elevated lateral stress where the maximum principal stress is in, or close to, the horizontal plane. Stylolite-related pores typically cross-cut bedding (Koehn *et al.* 2007, 2016; Ebner *et al.* 2010; Humphrey *et al.* 2019) (Fig. 4q, r) (Table 2). Stylolites have, in some cases, been reported to act as baffles to fluid flow (Bruna *et al.* 2019). For a stylolite to act as potential barrier to fluid flow, fine-grained material such as clay, organic matter or oxides need to occupy the uneven surfaces of the stylolite (Mehrabi *et al.* 2016; Bruna *et al.* 2019). However, it has also been suggested that some stylolites may contribute to porosity and lead to elevated permeability (Koehn *et al.* 2016). For example, when the sides of stylolite peaks are only partially filled with non-permeable materials, localized fluid can be trapped causing corrosion which leads to local secondary porosity generation (Koehn *et al.* 2016; Bruna *et al.* 2019).

Pore throats in mudstones

The size and character of pore throats are probably more significant for CCS projects than the size of pore bodies, as pore throats control the escape of CO_2 by capillary leakage or flow (Harding *et al.* 2018). Mudstones of a given porosity can have a wide range different mean pore throat size so that the latter requires attention (Yang and Aplin 2007).

Pore throats represent the narrowest gap between one pore and its neighbouring pore; pore throat size dictates how easily fluid can move from one pore to its neighbour. The classification of pore throats is distinct from the classification of pores bodies.

Pore throat size characterization is dependent on the measurement method employed (Nelson 2009). Mercury injection is a method routinely used to determine pore throat size. The Washburn equation

Downloaded from https://www.lyellcollection.org by University of Liverpool on Jan 26, 2023

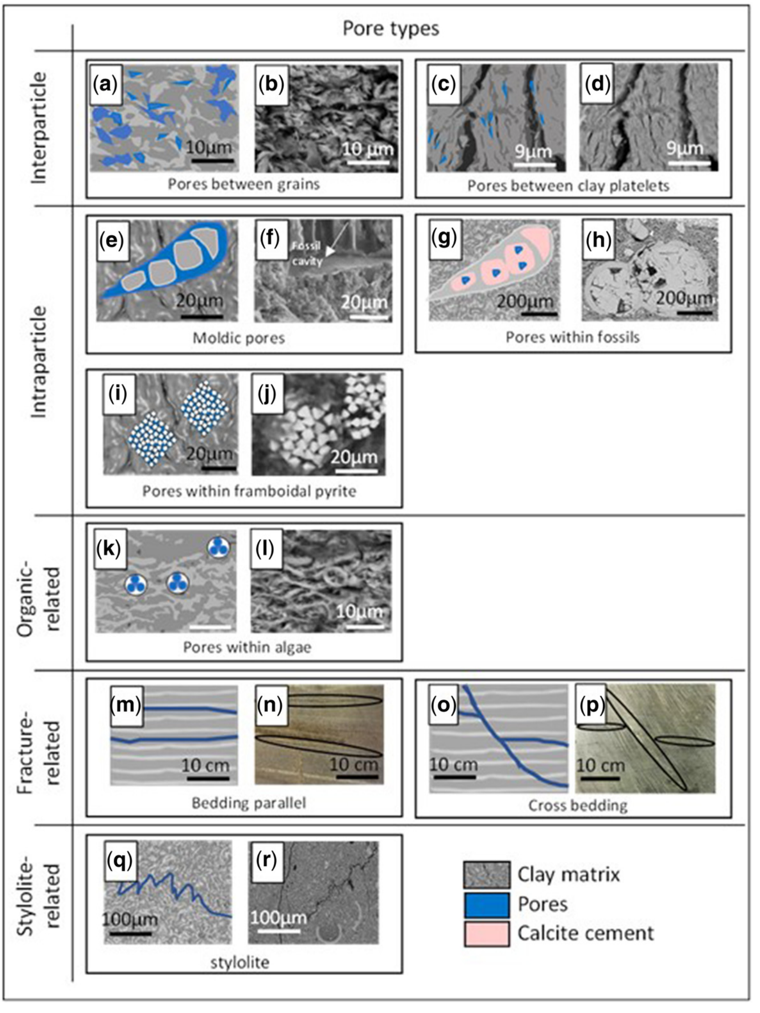

Fig. 4. Schematic illustration of pore body type classifications for mudstone top seals. (**a**, **b**) Interparticle pores between grains. (**c**, **d**) Intraparticle pores divided into three subcategories. (**e**, **f**) Moldic pores, for example fossil cavities. (**g**, **h**) Pores found within fossils body. (**i**, **j**) Pores formed within pyrite framboids. (**k**, **l**) Organic matter pores could be found within the body of boghead algae. (**m**, **n**) Fractures that formed parallel to bedding. (**o**, **p**) Pores linked to shear fractures. (**q**, **r**) Pores associated with stylolites. Note that (a), (c), (e), (g), (i), (k), (q) are schematic illustrations of the SEM–BSE images of (b), (d), (f), (h), (j), (r), whereas in fractures, (m) and (o) are schematic illustrations of the original image of the rock samples (n) and (p) (Peppers and Harvey 1997; Loucks *et al.* 2012; Koehn *et al.* 2016; Tiab and Donaldson 2016*b*).

is the typical method used to convert MICP data into pore throat diameter, requiring knowledge of interfacial tension and contact angle (Nelson 2009; Busch *et al.* 2017).

Pore throat classification in coal and siltstone

Zhang *et al.* (2020) argued that the IUPAC classification for pores and pore throat is not suitable for fine-grained sediments, despite its wide adoption in conventional and unconventional hydrocarbon studies (Rouquerol *et al.* 1994; Li *et al.* 2016). For example, if the IUPAC classification were applied to pore throats in mudstones, then all pore throats would be unhelpfully classified as macropores (Zhang *et al.* 2020).

Hodot (1966) proposed a classification scheme for pore throats in coal, and several authors adopted this classification (Li *et al.* 2012; Xin *et al.* 2019). The classification leads to several types of pore throats; (1) ultra-micropore throats (<2 nm), (2) micropore throats (2–10 nm), (3) transition pore

Downloaded from https://www.lyellcollection.org by University of Liverpool on Jan 26, 2023

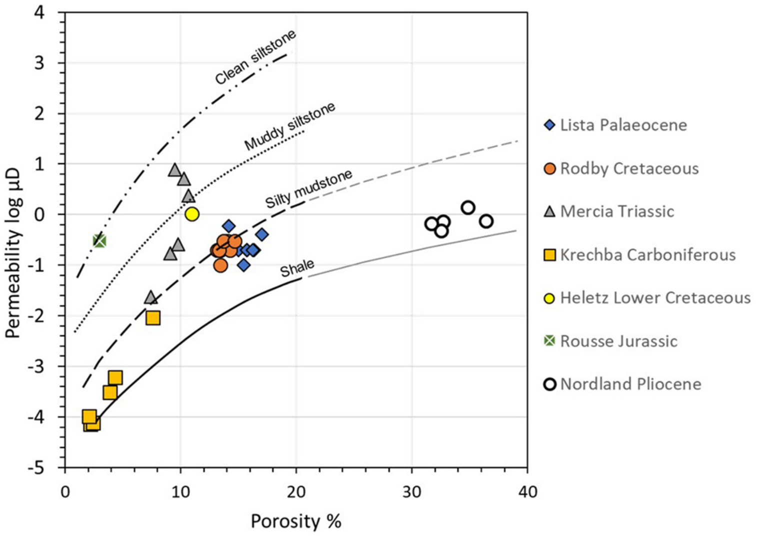

Fig. 5. Core-derived porosity data plotted against permeability in microdarcies from different CCS top-seals. The top-seals are from the (1) Rodby shale from the planned Acorn CCS site (Worden *et al.* 2020), (2) Lista shale from the planned East Mey CCS site (Worden *et al.* 2020) (3) Mercia Mudstone from the planned Hamilton CCS site (Armitage *et al.* 2013, 2016), (4) Carboniferous mudstones from the Krechba (In Salah) CCS site (Armitage *et al.* 2011), (5) Heletz CCS pilot site (Paluszny *et al.* 2020), (6) Peterhead from the planned Goldeneye CCS site (Paluszny *et al.* 2020), (7) Jurassic mudstones from the Rousse CCS pilot site (Tonnet *et al.* 2011), and (8) Pliocene Nordland Shale from Sleipner (Springer and Lindgren 2006). Published trends of porosity and permeability for fine-grained sediments have been used to compare the different top-seals (Neufelder *et al.* 2012) although the shale and silty mudstone trajectories have been extrapolated to help explain the Nordland shales from Sleipner which have high porosity but low permeability.

throats (10–100 nm), (4) mesopore throats (100 nm to 1 µm), (5) macropore throats (1–10 µm) and (6) microfractures (>10 µm). Zhang *et al.* (2020) updated the Hodot classification to make it applicable for tight siltstone reservoirs; the updated siltstone classification is (1) micropore throats (<10 nm), (2) transition pore throats (10–100 nm), (3) mesopore throats (100 nm to 0.625 µm), and (4) macropore throats (>0.625 µm).

Pore throat classification in mudstone

The classification of mean pore throat size in rocks is typically obtained from mercury intrusion porosimetry data (Nelson 2009; Busch *et al.* 2017; Worden *et al.* 2020). A pore throat classification scheme for CCS top seal mudstones has here been adopted from Zhang *et al.* (2020) as it seems to be suitable for CCS top seals.

Porosity–permeability and porosity–depth trends for mudstone top-seals from CCS sites

To better understand the effect of compaction and cementation on porosity-loss in top seals, a set of porosity–permeability values from different CCS sites is plotted on a porosity–permeability diagram (Fig. 6). The porosity of top-seals at CCS sites can vary over a wide range of values and yet still contain CO_2.

There are relatively few petrophysical properties published from CCS caprocks but porosity–permeability data are available from the Sleipner (Springer and Lindgren 2006), Heletz (Paluszny *et al.* 2020), Rousse (Tonnet *et al.* 2011) and Krechba (In Salah) (Armitage *et al.* 2011). Fields from planned CCS sites at Acorn, East Mey (Worden *et al.* 2020) and in the East Irish Sea (Armitage *et al.* 2016) (Fig. 5). Based on published data by Neufelder *et al.* (2012), porosity–permeability trend lines of different lithofacies types (shale, silty mudstone, muddy siltstone to clean siltstone) of fine-grained rocks have been added to the porosity–permeability diagram (Worden *et al.* 2020); here the trends from shale and silty mudstone have been extrapolated to help explain the data from the Nordland shale at Sleipner (Fig. 5). Weyburn top seal data have not been included in this plot as it is an evaporite seal and the main focus here is on clastic mudstones.

The porosity of the top-sealing mudstones tends to decrease with increasing age with the Pliocene Nordland shales having the highest porosity and

Downloaded from https://www.lyellcollection.org by University of Liverpool on Jan 26, 2023

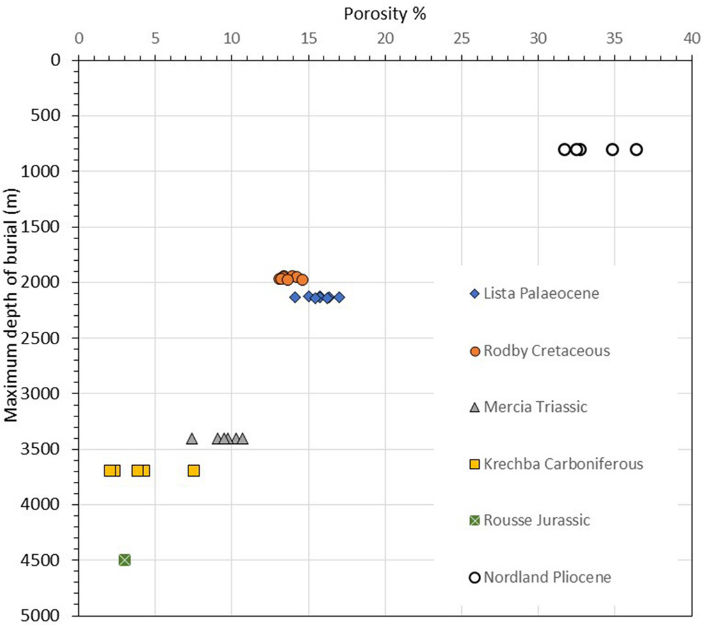

Fig. 6. Core-derived porosity data plotted against maximum depth from different CCS top-seals. The top seals are from the (1) Rodby Shale from the planned Acorn CCS site (Worden *et al.* 2020), (2) Lista Shale from the planned East Mey CCS site (Worden *et al.* 2020), (3) Mercia Mudstone from the planned Hamilton CCS site (Armitage *et al.* 2013, 2016), (4) Carboniferous mudstones from the Krechba (In Salah) CCS site (Armitage *et al.* 2010, 2011), (5) Jurassic mudstones from the Rousse CCS pilot site (Tonnet *et al.* 2011) and (6) Pliocene Nordland Shale from Sleipner (Springer and Lindgren 2006). There is a good relationship between maximum depth of burial and porosity, suggesting that porosity-loss is strongly controlled by increasing effective stress and temperature (and see Fig. 8).

the Carboniferous shales from Krechba (In Salah) having the lowest porosity (Fig. 5). The Paleocene Lista shales have slightly higher porosity than the Cretaceous Rodby shales and the Triassic Mercia Mudstones have porosity intermediate between the Cretaceous Rodby and Carboniferous Krechba shales. This pattern tends to suggest that compaction and porosity-loss is at least partly a function of age of mudstone, as has been reported from coarser-grained clastic rocks (Ehrenberg and Nadeau 2005).

The Jurassic Rousse sample has low porosity because it is calcite-rich and relatively siliceous (Tonnet *et al.* 2011). The Pliocene Nordland shale has very high porosity as it is relatively young and has not been buried to greater than about 800 m (Springer and Lindgren 2006). However, the permeability of the Nordland shale is relatively low for its high porosity; by reference to the extrapolated porosity–permeability trends this may be because it is less silty than many of the other clastic top-seals referred to here. Figure 5 demonstrates that it is necessary to develop an appreciation of mudstone lithofacies in order to relate top-seal porosity to permeability.

There is a good relationship between maximum depth of burial and porosity suggesting that porosity-loss is controlled by a combination of increasing effective stress and increasing temperature (Fig. 6). Maximum depth of burial is more significant than present day of burial; for example, if uplift has occurred, as it has for the Mercia (Armitage *et al.* 2013) and Krechba (Armitage *et al.* 2010) mudstones, then the porosity will seem to be lower than it should be for the present-day depth of burial. Permeability of these top-seals is a function of porosity although it also seems to depend on specific lithofacies. For example, some of the Mercia Mudstone samples have relatively high permeability for their porosity as they have been shown to be rich in silt (Armitage *et al.* 2016).

Genetic controls on the porosity of mudstones

Mudstone compaction

Porosity evolution in sedimentary rocks, including mudstone, is a result of the interplay between

Downloaded from https://www.lyellcollection.org by University of Liverpool on Jan 26, 2023

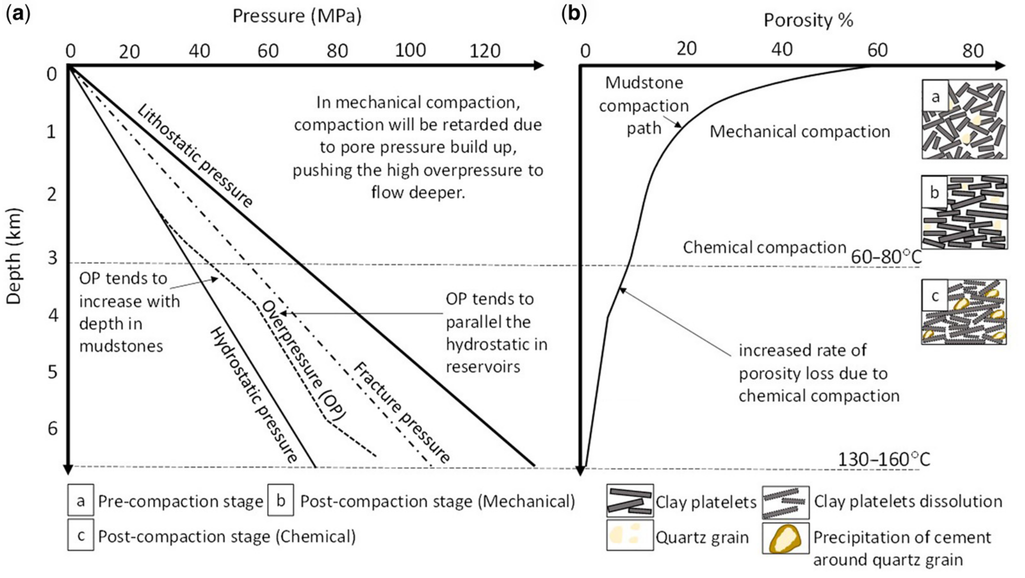

Fig. 7. (**a**) A profile of fluid and rock pressure v. depth for mudstones. The hydrostatic pressure gradient is a function of fluid density. If fluid pressure is greater than hydrostatic, then it is overpressured. If overpressure exceeds fracture pressure (σ_{hmin}, the minimum horizontal stress) than the rock will fail, allowing fluid pressure to dissipate. (**b**) Conceptual model of the evolution of mudstone porosity and the processes that drive porosity-reduction with depth (and compare to Fig. 7). Initially, mechanical compaction leads to porosity-reduction when rearrangements of grains and ductile deformation take place (a, b). If mudstones are overpressured then the elevated fluid pressure reduces the effective stress, reducing the degree of compaction and allowing porosity to be higher than it would be in equivalent hydrostatically pressured rocks. At greater depths and temperatures, porosity-loss is governed by chemical compaction involving mineral dissolution and recrystallization (c). (Bjorlykke and Hoeg 1997; Bjorlykke 1998; Charpentier *et al.* 2003; Sheldon *et al.* 2003; Worden *et al.* 2005; Day-Stirrat *et al.* 2010).

diagenetic and depositional processes (Armitage *et al.* 2010). The porosities of clay-rich sediment at the time of deposition ranges from 60 to 80% (Magara 1968; Dzevanshir *et al.* 1986; Armitage *et al.* 2010; Day-Stirrat *et al.* 2010) (Fig. 7). The initially elevated depositional porosity will be lost over time, during burial, because of the diagenetic processes of compaction and cementation (Armitage *et al.* 2010; Day-Stirrat *et al.* 2010).

Compaction includes mechanical and chemical processes that alter porosity, permeability, strength, volume, and density of the rock (Bjorlykke and Hoeg 1997; Bjorlykke 1998; Dutta 2002; Sheldon *et al.* 2003; Bjørlykke *et al.* 2010; Day-Stirrat *et al.* 2010; Lahann and Swarbrick 2011; Goulty *et al.* 2012, 2016). Fine-grained rocks, that are rich in clay minerals, have very high porosity (60% or more) at the time of deposition because the fine, sheet-like clay minerals have an open, 'house of cards'-type structure, in which the clay minerals are randomly aligned (Fig. 7). At the time of deposition, mud-rich sediments have higher porosity than well-sorted, clean sand-rich sediment. The initial stage of compaction (0 to *c.* 2000 m, up to 65–70°C) has a major impact on the porosity of fine-grained clastic rocks due to the rearrangement of the sheet-like clay minerals, from random alignment into sub-parallel alignment as vertical effective stress increases (Bjorlykke 1998; Charpentier *et al.* 2003; Worden *et al.* 2005; Day-Stirrat *et al.* 2010; Goulty *et al.* 2016) (Fig. 7). At elevated vertical effective stress and depths where the temperature exceeds 70–80°C, chemical processes commence; these include the process of chemical transformation of detrital clay minerals (e.g. smectite into illite) and chemically-enhanced dissolution (e.g. at mica–quartz interfaces) (Hedberg 1936; Day-Stirrat *et al.* 2010). In typical compactional regimes, compaction reduces the total volume of the rock by shortening as vertical effective stress increases (Hedberg 1936) (Fig. 7b).

There are different approaches to understanding the role of vertical effective stress in chemically-enhanced dissolution when mudstones reach depths where the temperature exceeds 70–80°C. Some consider that dissolution at quartz–mica interfaces is solely controlled by temperature and effective stress has no impact on the process (Bjorlykke and Hoeg 1997; Bjorlykke 1998). Others consider that vertical effective stress and temperature both

Downloaded from https://www.lyellcollection.org by University of Liverpool on Jan 26, 2023

play roles in dissolution at quartz–mica interfaces (Dutta 2002; Sheldon *et al.* 2003; Lahann and Swarbrick 2011; Goulty *et al.* 2016). This subtle difference is important since the former assigns no role to overpressure in controlling porosity-loss in mudstones, but the latter implies that reduced vertical effective stress, when the fluid pressure is overpressured, should lead to inhibited compaction and anomalously elevated porosity for the depth of burial (Fig. 7).

Overpressure

Hydrostatic pressure is the pressure exerted by the fluid column, typically water, at a given depth where the gradient is the result of the salinity-controlled density of the water (Bowers 2001, 2002). Oil and gas, with densities lower than water, lead to lower pressure gradients. Lithostatic pressure (also known as vertical effective stress or σ_v) is the pressure caused by bulk mineral density through grain-to-grain contacts; in extensional or quiescent basins σ_v is equivalent to σ_1, the maximum of the three orthogonal stress vectors. Rocks fracture when the pore fluid pressure exceeds the minimum stress vector, σ_3; in extensional basins this is the minimum horizontal stress (σ_{hmin}). The pressure at which rocks fail by shear is lower for rocks with pre-existing faults and fractures than intact rock (Sorkhabi 2014). Fracture pressure (σ_{hmin}, σ_3) is typically about 70–80% of the lithostatic pressure (σ_v, σ_1) (Yardley and Swarbrick 2000; Zoback 2007; Swarbrick and Lahann 2016; Udo *et al.* 2020). Overpressure, also known as abnormal pressure or geopressure, is where the fluid pressure exceeds the hydrostatic pressure (Bowers 2001, 2002; Velázquez-Cruz *et al.* 2017). Overpressure starts to develop during rapid burial when the fluid cannot rapidly escape from pores (Goulty 1998; Day-Stirrat *et al.* 2010) (Fig. 7a). If fluid pressure (overpressure) reaches the fracture pressure (σ_{hmin}) at any given depth, then the rock will fail, allowing the high-pressure fluid to dissipate.

Causes of overpressure

Overpressure can be caused by a number of processes such as: (1) progressive burial of low permeability sediment (e.g. mudstone), from which the pore fluid cannot easily escape and so fluid pressure builds up (Goulty 1998; Dutta 2002; Lahann and Swarbrick 2011; Goulty *et al.* 2012); this is known as disequilibrium compaction; (2) conversion of hydroxyl-rich smectite into high temperature hydroxyl-poor clay such as illite or chlorite, creating new water that contributes to fluid pressure (Burst 1969; Harrison and Summa 1991; Lahann and Swarbrick 2011); (3) conversion of kerogen to oil or gas (especially in mudstones with high total organic carbon) (Meissner 1981; Spencer 1987; Lahann and Swarbrick 2011). Mudstones are commonly rich in smectite at the time of deposition so that mechanism 2 is likely to be common. The ease of escape of fluid being squeezed out of mudstones depends on details of the stratigraphy, and occurrence of transmissible faults (Magara 1968; Xinong *et al.* 1999). Natural hydrofracturing of mudstones is a common consequence of disequilibrium compaction (Magara 1968; Wang and Xie 1998; Xinong *et al.* 1999).

Effect of injected CO_2 on mudstone top-seals

Capillary sealing limits

Lithology is a paramount factor that influences the effectiveness of top seals (Ingram and Urai 1999). An ideal top-seal is ductile, and thus self-sealing, has low permeability and high capillary entry pressure, and is largely laterally and stratigraphically homogenous (Rutqvist 2012). Mudstones routinely act as top-seals to hydrocarbon columns, as evidenced by countless oil and gas fields. This phenomenon can be explained by the theory of capillary sealing and capillary entry pressure (Watts 1987). It has been assumed that a sealing rock that has the ability to retain a hydrocarbon column should also be able to support a CO_2 column (Rutqvist 2012; Kaldi *et al.* 2013).

Fluid pressure, induced fractures, and the orientation of the regional stress regime in comparison to the orientation of pre-existing fractures, collectively control the geomechanical properties of a caprock (Kaldi *et al.* 2013). An increase in fluid pressure due to CO_2 injection will influence the efficacy of a top-seal. Knowledge of the geomechanical properties of a caprock is important for seal integrity (Kaldi *et al.* 2013). When CO_2 is injected, the increased fluid pressure could cause seal damage, mechanical deformation, new (induced) fractures (Fig. 8), and reactivation of pre-existing faults and fractures (Kaldi *et al.* 2013). New microfractures and slip on existing faults can be triggered when CO_2 is injected; this has been evidenced by microseismic activity linked to high rates of CO_2 injection, especially in low permeability reservoirs (Payre *et al.* 2014; Stork *et al.* 2015). Microfractures might open rapidly during initial CO_2 injection but they may also close following injection and dissipation of fluid pressure (Kaldi *et al.* 2013) (Fig. 8).

The integrity of a mudstone top-seal to injected CO_2

The integrity of a top-seal to a CO_2 storage site is influenced by a combination of interlinked geochemical, geomechanical, and petrophysical attributes of the mudstones (Worden *et al.* 2020).

Downloaded from https://www.lyellcollection.org by University of Liverpool on Jan 26, 2023

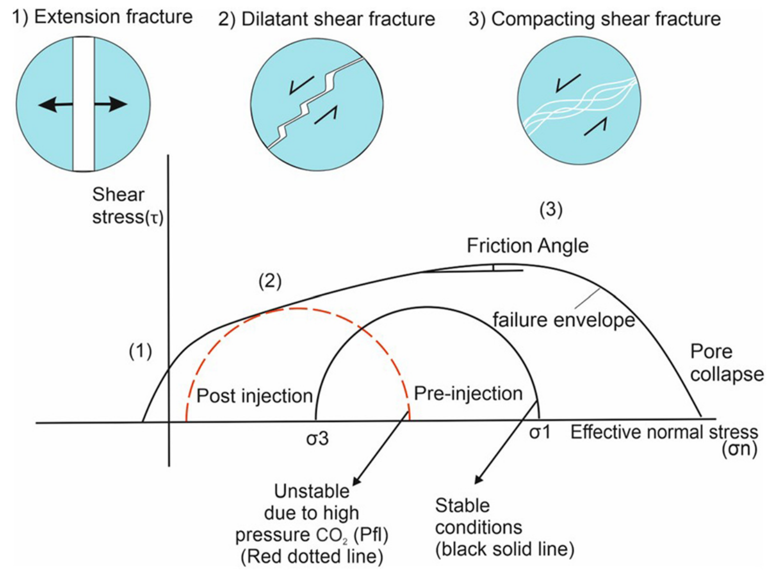

Fig. 8. Three modes of fracture deformation on a Mohr diagram with the injection of CO_2. Before injection, the position of the circle represents stable conditions. When the circle moves to the left due to high (CO_2) fluid pressure (P_{fl}), it may touch the failure envelope and the rock then becomes unstable. Extensional fractures (1) are the result of tensile failure (normal stress regime). Extension fracture formation is reliant on the position and size of the Mohr circle. Dilatant shear fractures (2) form in rocks in a low confining stress regime during deformation and when the friction is high, which corresponds to strong rocks. Compacting shear fractures (3) develop during deep burial when the confining pressure is high during rock deformation or when the friction angle is low during the deformation of weak ductile rocks. Compacting shear fractures are the only ones that tend to remain closed and sealed after deformation. Source: modified after Ingram and Urai (1999).

There is a possible sequence of events that may affect the integrity of a top seal when CO_2 is injected (Fig. 9). For instance: initially (step 1) CO_2 pressure rises in the reservoir, and then (step 2) a gradient in CO_2 partial pressure (Pco_2) develops at the base of the top-seal mudstone (Espinoza and Santamarina 2012). Next (step 3), high fluid pressure may lead to localized fracturing of the top-seal, especially if the mudstone is brittle (i.e. rich in quartz silt), the new fractures may lead to elevated exposed surface area enabling CO_2-top-seal interaction (Rutqvist 2012). High pressure CO_2 may exceed the capillary entry pressure (step 4) and start to penetrate the top-seal mudstone (Worden *et al.* 2020). After that, formation brine in the mudstone will become acidified by the high-pressure CO_2 (step 5), possibly leading to dissolution of calcite and other carbonates (e.g. dolomite, siderite) and replacement of reactive clay minerals such as chlorite (Espinoza and Santamarina 2012). The dissolution of minerals will increase porosity and permeability and may weaken the rock, promoting additional geomechanical damage (Worden *et al.* 2020). The anhydrous CO_2 may allow the H_2O from brine in mudstone pores to evaporate (step 6) leading to increasingly saline pore waters (Miri and Hellevang 2016). If pore waters become sufficiently saturated, then halite precipitation may commence serving to block pores and pore throats in mudstones (Miri and Hellevang 2016) (Fig. 9).

CO_2 sorption on clay minerals and grain surfaces

The process of CO_2 sorption on minerals in sedimentary rocks is complicated by the diversity of minerals and their pre-CO_2 exposure history (Jeon *et al.* 2014). Some research has focused on the physical interactions between clay minerals and CO_2, with the objective of understanding the response of clay minerals to contact with CO_2 (Busch *et al.* 2016). While interesting, some of these studies have limited applicability as they did not account for the effect of elevated pressure and temperature (>10 MPa, >40° C) within CO_2 reservoirs and their overlying top-seal mudstones (Busch *et al.* 2016).

The phenomenon of the adsorption of gas on micropore surfaces is well documented and play a key role in shale gas production and coal bed methane (Busch *et al.* 2010). A direct positive correlation was found between total organic carbon (TOC) and

Downloaded from https://www.lyellcollection.org by University of Liverpool on Jan 26, 2023

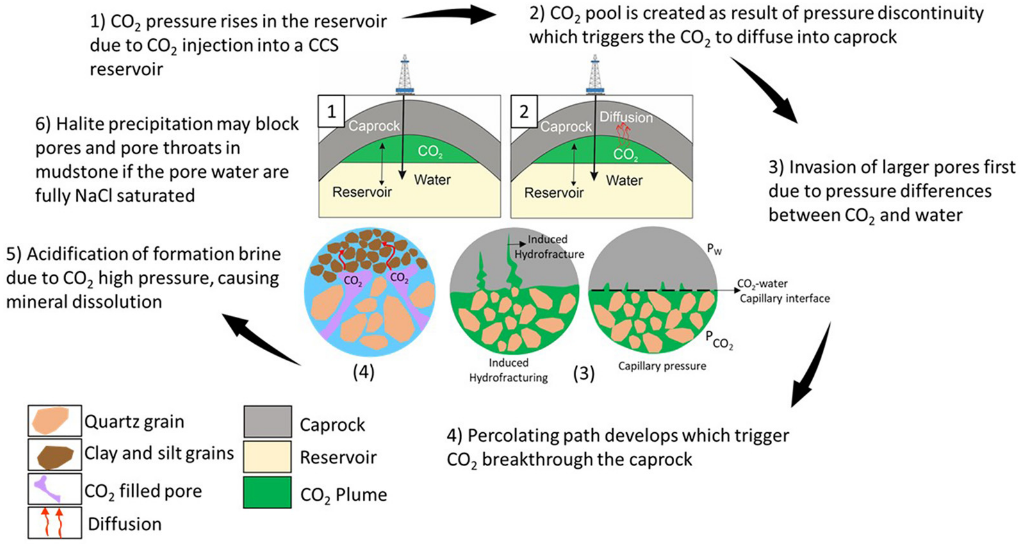

Fig. 9. A schematic representation of the possible sequence of events that could occur during the invasion of injected CO_2 into the caprock (Espinoza and Santamarina 2012; Rutqvist 2012; Miri and Hellevang 2016; Worden *et al.* 2020).

CO_2 storage capacity suggesting that CO2 can be absorbed by solid organic carbon compounds within mudstone (Busch *et al.* 2008, 2010). Another correlation was found between the Brunauer–Emmett–Teller BET surface area analysis by N_2 and CO_2 sorption, and micropore clay volume (Venaruzzo *et al.* 2002).

Some clay minerals can absorb a significant amount of CO_2 (Busch *et al.* 2008). In decreasing order of absorption capacity: Ca-rich smectite has largest absorption capacity, followed by Na-rich smectite, kaolinite, illite, and, last of all, chlorite (Busch *et al.* 2008, 2016). The CO_2 absorbed into smectite sits between the (001) tetrahedral–octahedral–tetrahedral sheets and causes the crystal structure to change (expand) compared to the dehydrated state (Loring *et al.* 2019; Zhang and Wu 2019). CO_2 absorption into smectite can causes the mineral to swell (strain) by at least 2% (Zhang and Wu 2019). This process may serve as a way to physically lock away CO_2 and to help better seal up any natural or induced fractures in smectite-rich top-seal mudstones.

Conclusions

(1) The distinctive petrophysical and geomechanical characteristics of mudstone play a key role in sealing CO_2 in CCS sites through different kinds of structural and stratigraphic trapping.

(2) Seal integrity, potential, capacity, and geometry are key factors for evaluating top seal effectiveness in mudstone.

(3) Pores (pore bodies) in mudstone top-seals at carbon capture and storage sites are likely to be in the range between (<62 µm–1 nm).

(4) Pores in mudstones have a range of origins: interparticle pores, which are pores formed between grain or between clay platelets; intraparticle pores, which includes moldic pores, organic matter pores, and fractures.

(5) Pore throats for mudstone top seals at carbon capture and storage sites are categorized here as (1) macropore throats (>0.625 µm), (2) mesopore throats (0.1–0.625 µm), (3) transitional pore throats (10 nm to 0.1 µm), (4) nanopore throats (<10 nm).

(6) The processes of mechanical and chemical compaction alter mudstone porosity with depth. At the initial stage of mechanical compaction (0 to *c.* 2000 m, up to 65–70°C), rearrangement of clay sheets into an increasingly compact arrangement drives porosity-reduction. At greater depths and elevated vertical effective stress, and where the temperature exceeds 80°C, chemical compaction commences and leads to the transformation and dissolution of clays and other minerals.

(7) Younger top-seal mudstones tend to have higher porosity than older mudstones. Permeability of mudstones decreases with decreasing porosity but mudstone lithofacies plays

Downloaded from https://www.lyellcollection.org by University of Liverpool on Jan 26, 2023

an important role with increasing grain size (silt content) leading to relatively higher permeability.

(8) Porosity-reduction can be inhibited by the development of overpressure. There are several causes of overpressure such as rapid burial, conversion of smectite into high temperature illite, and conversion of kerogen into oil or gas.

(9) High fluid pressure due to the injected CO_2 can damage the seal and cause mechanical deformation, fractures, microfractures, and fault reactivation.

(10) The integrity of a mudstone top seal is controlled by a combination of geochemical and geomechanical processes that influence petrophysical properties.

(11) The process of CO_2 sorption on clay minerals and grain surface is complex due to mineral diversity and their history of pre-CO_2 exposure. Smectite can absorb CO_2 and consequently increase in volume, possibly reducing pore throat sizes and adding to sealing capacity.

Competing interests The authors declare that they have no known competing financial interests or personal relationships that could have appeared to influence the work reported in this paper.

Author contributions **NA**: data curation (lead), formal analysis (lead), visualization (lead), writing – original draft (lead); **RHW**: supervision (lead), writing – review & editing (lead).

Funding This research received no specific grant from any funding agency in the public, commercial, or not-for-profit sectors.

Data availability All data generated or analysed during this study are included in this published article (and its supplementary information files).

References

Ajayi, T., Gomes, J.S. and Bera, A. 2019. A review of CO_2 storage in geological formations emphasizing modeling, monitoring and capacity estimation approaches. *Petroleum Science*, **16**, 1028–1063, https://doi.org/10.1007/s12182-019-0340-8

Alcalde, J., Heinemann, N. *et al*. 2019. Developing full-chain industrial carbon capture and storage in a resource- and infrastructure-rich hydrocarbon province. *Journal of Cleaner Production*, **233**, 963–971, https://doi.org/10.1016/j.jclepro.2019.06.087

Aplin, A.C. and Macquaker, J.H.S. 2011. Mudstone diversity: Origin and implications for source, seal, and reservoir properties in petroleum systems. *American Association of Petroleum Geologist Bulletin*, **95**, 2031–2059, https://doi.org/10.1306/03281110162

Armitage, P.J., Worden, R.H., Faulkner, D.R., Aplin, A.C., Butcher, A.R. and Iliffe, J. 2010. Diagenetic and sedimentary controls on porosity in Lower Carboniferous fine-grained lithologies, Krechba Field, Algeria: a petrological study of a caprock to a carbon capture site. *Marine and Petroleum Geology*, **27**, 1395–1410, https://doi.org/10.1016/j.marpetgeo.2010.03.018

Armitage, P.J., Faulkner, D.R., Worden, R.H., Aplin, A.C., Butcher, A.R. and Iliffe, J. 2011. Experimental measurement of, and controls on, permeability and permeability anisotropy of caprocks from the CO_2 storage project at the Krechba Field, Algeria. *Journal of Geophysical Research*, **116**, https://doi.org/10.1029/2011jb008385

Armitage, P.J., Worden, R.H., Faulkner, D.R., Aplin, A.C., Butcher, A.R. and Espie, A.A. 2013. Mercia Mudstone Formation caprock to carbon capture and storage sites: petrology and petrophysical characteristics. *Journal of the Geological Society, London*, **170**, 119–132, https://doi.org/10.1144/jgs2012-049

Armitage, P.J., Worden, R.H., Faulkner, D.R., Butcher, A.R. and Espie, A.A. 2016. Permeability of the Mercia Mudstone: suitability as caprock to carbon capture and storage sites. *Geofluids*, **16**, 26–42, https://doi.org/10.1111/gfl.12134

Bjorlykke, K. 1998. Clay mineral diagenesis in sedimentary basins. A key to the prediction of rock properties. Examples from the North Sea Basin. *Clay Minerals*, **33**, 15–34, https://doi.org/10.1180/00098559854 5390

Bjorlykke, K. and Hoeg, K. 1997. Effects of burial diagenesis on stresses, compaction and fluid flow in sedimentary basins. *Marine and Petroleum Geology*, **14**, 267–276, https://doi.org/10.1016/S0264-8172(96)00051-7

Bjørlykke, K., Jahren, J., Aagaard, P. and Fisher, Q. 2010. Role of effective permeability distribution in estimating overpressure using basin modelling. *Marine and Petroleum Geology*, **27**, 1684–1691, https://doi.org/10.1016/j.marpetgeo.2010.05.003

Bowers, G.L. 2001. Determining an appropriate pore-pressure estimation strategy. Paper presented at the Offshore Technology Conference, 30 April–3 May Houston, Texas.

Bowers, G.L. 2002. Detecting high overpressure. *The Leading Edge*, **21**, 174–177, https://doi.org/10.1190/1.1452608

Bruna, P.O., Lavenu, A.P.C., Matonti, C. and Bertotti, G. 2019. Are stylolites fluid-flow efficient features? *Journal of Structural Geology*, **125**, 270–277, https://doi.org/10.1016/j.jsg.2018.05.018

Burst, J. 1969. Diagenesis of the Gulf Coast clayey sediments and its possible relation to petroleum migration. *American Association of Petroleum Geologist Bulletin*, **53**, 73–93.

Busch, A. and Amann-Hildenbrand, A. 2013. Predicting capillarity of mudrocks. *Marine and Petroleum Geology*, **45**, 208–223, https://doi.org/10.1016/j.marpetgeo.2013.05.005

Busch, A., Alles, S. *et al*. 2008. Carbon dioxide storage potential of shales. *International Journal of Greenhouse Gas Control*, **2**, 297–308, https://doi.org/10.1016/j.ijggc.2008.03.003

Downloaded from https://www.lyellcollection.org by University of Liverpool on Jan 26, 2023

Busch, A., Amann, A., Bertier, P., Waschbusch, M. and Krooss, B.M. 2010. The significance of caprock sealing integrity for CO_2 storage. SPE International Conference on CO_2 Capture, Storage, and Utilization, New Orleans, Louisiana.

Busch, A., Bertier, P., Gensterblum, Y., Rother, G., Spiers, C.J., Zhang, M. and Wentinck, H.M. 2016. On sorption and swelling of CO_2 in clays. *Geomechanics and Geophysics for Geo-Energy and Geo-Resources*, **2**, 111–130, https://doi.org/10.1007/s40948-016-0024-4

Busch, A., Schweinar, K. *et al*. 2017. Determining the porosity of mudrocks using methodological pluralism. *Geological Society, London, Special Publications*, **454**, 15–38, https://doi.org/10.1144/sp454.1

Cardott, B.J. and Curtis, M.E. 2018. Identification and nanoporosity of macerals in coal by scanning electron microscopy. *International Journal of Coal Geology*, **190**, 205–217, https://doi.org/10.1016/j.coal.2017.07.003

Charpentier, D., Worden, R.H., Dillon, C.G. and Aplin, A.C. 2003. Fabric development and the smectite to illite transition in Gulf of Mexico mudstones: an image analysis approach. *Journal of Geochemical Exploration*, **78–79**, 459–463, https://doi.org/10.1016/S0375-6742(03)00073-6

Choquette, P.W. and Pray, L.C. 1970. Geological nomenclature and classification of porosity in sedimentary carbonates. *American Association of Petroleum Geologists Bulletin*, **54**, 207–250.

Curtis, M.E., Sondergeld, C.H., Ambrose, R.J. and Rai, C.S. 2012. Microstructural investigation of gas shales in two and three dimensions using nanometer-scale resolution imaging. *American Association of Petroleum Geologist Bulletin*, **96**, 665–677, https://doi.org/10.1306/08151110188

Day-Stirrat, R.J., McDonnell, A. and Wood, L.J. 2010. Diagenetic and seismic concerns associated with interpretation of deeply buried 'mobile shales'. *American Association of Petroleum Geologists Memoir*, **93**, 5–27, https://doi.org/10.1306/13231306m93730

Dernaika, M., Walls, J., Koronfol, S. and Al Jallad, O. 2017. Petrophysical Properties of Shale From Different Source Rocks in the Middle East. Proceedings of the 5th Unconventional Resources Technology Conference, 24–26 July, Austin, Texas.

Desbois, G., Urani, J.L. and Kukla, P.A. 2009. Morphology of the pore space in claystones – evidence from BIB/FIB ion beam sectioning and cryo-SEM observations. *eEarth*, **4**, 15–22, https://doi.org/10.5194/ee-4-15-2009

Dewhurst, D., Jones, R. and Raven, M. 2002. Microstructural and petrophysical characterization of Muderong Shale: application to top seal risking. *Petroleum Geoscience*, **8**, 371–383, https://doi.org/10.1144/petgeo.8.4.371

Divko, L.G., Hamilton, J. and O'Brien, G.W. 2010. Evaluation of the regional top seal for the purpose of geological sequestration on the Gippsland Basin, Southern Australia. *Search and Discovery*, article #80099.

Dutta, N.C. 2002. Deepwater geohazard prediction using prestack inversion of large offset P-wave data and rock model. *The Leading Edge*, **21**, 193–198, https://doi.org/10.1190/1.1452612.

Dzevanshir, R.D., Buryakovskiy, L.A. and Chilingarian, G.V. 1986. Simple quantitative evaluation of pororsity of argillaceous sediments at various depths of burial. *Sedimentary Geology*, **46**, 169–175, https://doi.org/10.1016/0037-0738(86)90057-6

Ebner, M., Piazolo, S., Renard, F. and Koehn, D. 2010. Stylolite interfaces and surrounding matrix material: nature and role of heterogeneities in roughness and microstructural development. *Journal of Structural Geology*, **32**, 1070–1084, https://doi.org/10.1016/j.jsg.2010.06.014

Ehrenberg, S.N. and Nadeau, P.H. 2005. Sandstone v. carbonate petroleum reservoirs: a global perspective on porosity–depth and porosity–permeability relationships. *American Association of Petroleum Geologists Bulletin*, **89**, 435–445, https://doi.org/10.1306/11230404071

Espinoza, D.N. and Santamarina, J.C. 2012. Clay interaction with liquid and supercritical CO_2: the relevance of electrical and capillary forces. *International Journal of Greenhouse Gas Control*, **10**, 351–362, https://doi.org/10.1016/j.ijggc.2012.06.020

Espinoza, D.N. and Santamarina, J.C. 2017. CO_2 breakthrough – Caprock sealing efficiency and integrity for carbon geological storage. *International Journal of Greenhouse Gas Control*, **66**, 218–229, https://doi.org/10.1016/j.ijggc.2017.09.019

Ewy, R.T. 2015. Shale/claystone response to air and liquid exposure, and implications for handling, sampling and testing. *International Journal of Rock Mechanics and Mining Sciences*, **80**, 388–401, https://doi.org/10.1016/j.ijrmms.2015.10.009

Gluyas, J. 2005. Sedimentary rocks | Sandstones, diagenesis and porosity evolution. *In*: Selley, R.C., Cocks, R.M. and Plimer, I.R. (eds) *Encyclopedia of Geology*. Elsevier, 141–151.

Goulty, N.R. 1998. Relationships between porosity and effective stress in shales. *First Break*, **16**, 413–419, https://doi.org/10.1046/j.1365-2397.1998.00698.x

Goulty, N.R., Ramdhan, A.M. and Jones, S.J. 2012. Chemical compaction of mudrocks in the presence of overpressure. *Petroleum Geoscience*, **18**, 471–479, https://doi.org/10.1144/petgeo2012-018

Goulty, N.R., Sargent, C., Andras, P. and Aplin, A.C. 2016. Compaction of diagenetically altered mudstones – Part 1: mechanical and chemical contributions. *Marine and Petroleum Geology*, **77**, 703–713, https://doi.org/10.1016/j.marpetgeo.2016.07.015

Harding, F.C., James, A.T. and Robertson, H.E. 2018. The engineering challenges of CO_2 storage. *Proceedings of the Institution of Mechanical Engineers, Part A: Journal of Power and Energy*, **232**, 17–26, https://doi.org/10.1177/0957650918756542

Harrison, W. and Summa, L. 1991. Paleohydrology of the Gulf of Mexico Basin. *American Journal of Science*, **291**, 109–176, https://doi.org/10.2475/ajs.291.2.109

Hedberg, H.D. 1936. Gravitional compaction of clays and shales. *American Journal of Science*, **31**, 241–287, https://doi.org/10.2475/ajs.s5-31.184.241

Hellevang, H., Pham, V.T.H. and Aagaard, P. 2013. Kinetic modelling of CO_2-water-rock interactions. *International Journal of Greenhouse Gas Control*, **15**, 3–15, https://doi.org/10.1016/j.ijggc.2013.01.027

Hildenbrand, A., Schlomer, S., Krooss, B. and Littke, R. 2004. Gas breakthrough experiments on pelitic rocks: comparative study with N_2, CO_2 and CH_4. *Geofluids*,

Downloaded from https://www.lyellcollection.org by University of Liverpool on Jan 26, 2023

4, 61–80, https://doi.org/10.1111/j.1468-8123.2004.00073.x
Hodot, B.B. 1966. *Outburst of Coal and Coalbed Gas (Chinese Translation)*. China Coal Industry Press, Beijing.
Humphrey, E., Gomez-Rivas, E., Koehn, D., Bons, P.D., Neilson, J., Martín-Martín, J.D. and Schoenherr, J. 2019. Stylolite-controlled diagenesis of a mudstone carbonate reservoir: a case study from the Zechstein_2_ Carbonate (Central European Basin, NW Germany). *Marine and Petroleum Geology*, **109**, 88–107, https://doi.org/10.1016/j.marpetgeo.2019.05.040
Ingram, G.M. and Urai, J.L. 1999. Top-seal leakage through faults and fractures: the role of mudrock properties. *Geological Society, London, Special Publications*, **158**, 125–135, https://doi.org/10.1144/GSL.SP.1999.158.01.10
IPCC 2005. *Special Report on Carbon Dioxide Capture and Storage*. Cambridge University Press.
Jarvie, D.M., Hill, R.J., Ruble, T.E. and Pollastro, R.M. 2007. Unconventional shale-gas systems: the Mississippian Barnett Shale of north-central Texas as one model for thermogenic shale-gas assessment. *American Association of Petroleum Geologist Bulletin*, **91**, 475–499, https://doi.org/10.1306/12190606068
Jeon, P.R., Choi, J., Yun, T.S. and Lee, C.-H. 2014. Sorption equilibrium and kinetics of CO2 on clay minerals from subcritical to supercritical conditions: CO2 sequestration at nanoscale interfaces. *Chemical Engineering Journal*, **255**, 705–715, https://doi.org/10.1016/j.cej.2014.06.090
Kaldi, J.G., Daniel, R.F. *et al*. 2011. *Caprock Systems for Geological Storage of CO_2*. Cooperative Research Centre for Greenhouse Gas Technologies.
Kaldi, J., Daniel, R. *et al*. 2013. Containment of CO_2 in CCS: role of caprocks and faults. *Energy Procedia*, **37**, 5403–5410, https://doi.org/10.1016/j.egypro.2013.06.458
Kampman, N., Busch, A. *et al*. 2016. Observational evidence confirms modelling of the long-term integrity of CO_2-reservoir caprocks. *Nature Communications*, **7**, 12268, https://doi.org/10.1038/ncomms12268
Koehn, D., Renard, F., Toussaint, R. and Passchier, C. 2007. Growth of stylolite teeth patterns depending on normal stress and finite compaction. *Earth and Planetary Science Letters*, **257**, 582–595, https://doi.org/10.1016/j.epsl.2007.03.015
Koehn, D., Rood, M.P., Beaudoin, N., Chung, P., Bons, P.D. and Gomez-Rivas, E. 2016. A new stylolite classification scheme to estimate compaction and local permeability variations. *Sedimentary Geology*, **346**, 60–71, https://doi.org/10.1016/j.sedgeo.2016.10.007
Krevor, S., Blunt, M.J., Benson, S.M., Pentland, C.H., Reynolds, C., Al-Menhali, A. and Niu, B. 2015. Capillary trapping for geologic carbon dioxide storage – from pore scale physics to field scale implications. *International Journal of Greenhouse Gas Control*, **40**, 221–237, https://doi.org/10.1016/j.ijggc.2015.04.006
Kwon, O., Kronenberg, A.K., Gangi, A.F., Johnson, B. and Herbert, B.E. 2004. Permeability of illite-bearing shale: 1. Anisotropy and effects of clay content and loading. *Journal of Geophysical Research: Solid Earth*, **109**, https://doi.org/10.1029/2004jb003052
Lahann, R.W. and Swarbrick, R.E. 2011. Overpressure generation by load transfer following shale framework weakening due to smectite diagenesis. *Geofluids*, **11**, 362–375, https://doi.org/10.1111/j.1468-8123.2011.00350.x
Li, S., Tang, D., Xu, H. and Yang, Z. 2012. Advanced characterization of physical properties of coals with different coal structures by nuclear magnetic resonance and X-ray computed tomography. *Computers & Geosciences*, **48**, 220–227, https://doi.org/10.1016/j.cageo.2012.01.004
Li, A., Ding, W., He, J., Dai, P., Yin, S. and Xie, F. 2016. Investigation of pore structure and fractal characteristics of organic-rich shale reservoirs: a case study of Lower Cambrian Qiongzhusi formation in Malong block of eastern Yunnan Province, South China. *Marine and Petroleum Geology*, **70**, 46–57, https://doi.org/10.1016/j.marpetgeo.2015.11.004
Lohr, C.D. and Hackley, P.C. 2018. Using mercury injection pressure analyses to estimate sealing capacity of the Tuscaloosa marine shale in Mississippi, USA: implications for carbon dioxide sequestration. *International Journal of Greenhouse Gas Control*, **78**, 375–387, https://doi.org/10.1016/j.ijggc.2018.09.006
Loring, J.S., Miller, Q.R.S., Thompson, C.J. and Schaef, H.T. 2019. Experimental studies of reactivity and transformations of rocks and minerals in water-bearing supercritical CO_2. *In*: Newell, P. and Ilgen, A.G (eds) *Science of Carbon Storage in Deep Saline Formations*. Elsevier, 63–88.
Loucks, R.G., Reed, R.M., Ruppel, S.C. and Jarvie, D.M. 2009. Morphology, genesis, and distribution of nanometer-scale pores in siliceous mudstones of the Mississippian Barnett Shale. *Journal of Sedimentary Research*, **79**, 848–861, https://doi.org/10.2110/jsr.2009.092
Loucks, R.G., Reed, R.M., Ruppel, S.C. and Hammes, U. 2012. Spectrum of pore types and networks in mudrocks and a descriptive classification for matrix-related mudrock pores. *American Association of Petroleum Geologist Bulletin*, **96**, 1071–1098, https://doi.org/10.1306/08171111061
Lu, J., Milliken, K., Reed, R.M. and Hovorka, S. 2011. Diagenesis and sealing capacity of the middle Tuscaloosa mudstone at the Cranfield carbon dioxide injection site, Mississippi, USA. *Environmental Geosciences*, **18**, 35–53, https://doi.org/10.1306/eg.09091010015
Ma, L., Fauchille, A., Dowey, P.J., Figueroa Pilz, F., Courtois, L., Taylor, K.G. and Lee, P.D. 2017. Correlative multi-scale imaging of shales: a review and future perspectives. *Geological Society, London, Special Publications*, **454**, 175–199, https://doi.org/10.1144/sp454.11
Magara, K. 1968. Compaction and migration of fluids in Miocene Mudstone Nagaoka Plain, Japan. *American Association of Petroleum Geologists Bulletin*, **52**, 2466–2501.
Mehrabi, H., Mansouri, M., Rahimpour-Bonab, H., Tavakoli, V. and Hassanzadeh, M. 2016. Chemical compaction features as potential barriers in the Permian-Triassic reservoirs of Southern Iran. *Journal of Petroleum Science and Engineering*, **145**, 95–113, https://doi.org/10.1016/j.petrol.2016.03.020
Meissner, F. 1981. Abnormal pressures produced by hydrocarbon generation and maturation and their relation to

Downloaded from https://www.lyellcollection.org by University of Liverpool on Jan 26, 2023

processes of migration and accumulation. *American Association of Petroleum Geologist Bulletin*, **65**, 2467–2467, https://doi.org/10.1306/03B599E0-16D1-11D7-8645000102C1865D

Miri, R. and Hellevang, H. 2016. Salt precipitation during CO2 storage – a review. *International Journal of Greenhouse Gas Control*, **51**, 136–147, https://doi.org/10.1016/j.ijggc.2016.05.015

Nelson, P.H. 2009. Pore-throat sizes in sandstones, tight sandstones, and shales. *American Association of Petroleum Geologist Bulletin*, **93**, 329–340, https://doi.org/10.1306/10240808059

Neufelder, R.J., Bowen, B.B., Lahann, R.W. and Rupp, J.A. 2012. Lithologic, mineralogical, and petrophysical characteristics of the Eau Claire Formation: complexities of a carbon storage system seal. *Environmental Geosciences*, **19**, 81–104, https://doi.org/10.1306/eg.02081211014

Paluszny, A., Graham, C.C. *et al*. 2020. Caprock integrity and public perception studies of carbon storage in depleted hydrocarbon reservoirs. *International Journal of Greenhouse Gas Control*, **98**, https://doi.org/10.1016/j.ijggc.2020.103057

Passey, Q.R., Bohacs, K.M., Esch, W.L., Klimentidis, R. and Sinha, S. 2010. From oil-prone source rock to gas-producing shale reservoir – geologic and petrophysical characterization of unconventional shale-gas reservoirs. CPS/SPE International Oil & Gas Conference, Beijing, China.

Payre, X., Maisons, C., Marble, A. and Thibeau, S. 2014. Analysis of the passive seismic monitoring performance at the Rousse CO_2 storage demonstration pilot. *Energy Procedia*, **63**, 4339–4357, https://doi.org/10.1016/j.egypro.2014.11.469

Peng, S., Zhang, T., Loucks, R.G. and Shultz, J. 2017. Application of mercury injection capillary pressure to mudrocks: conformance and compression corrections. *Marine and Petroleum Geology*, **88**, 30–40, https://doi.org/10.1016/j.marpetgeo.2017.08.006

Peppers, R.A. and Harvey, R.D. 1997. *Distribution of Boghead Algae in Illinois Basin Coral Beds*. Illinois State Geological Survey.

Polakowski, C., Ryżak, M., Sochan, A., Beczek, M., Mazur, R. and Bieganowski, A. 2021. Particle size distribution of various soil materials measured by laser diffraction – the problem of reproducibility. *Minerals*, **11**, https://doi.org/10.3390/min11050465

Ringrose, P. 2020. *How to Store CO_2 Underground: Insights from Early-Mover CCS Projects*. Springer.

Rouquerol, J., Avnir, D. *et al*. 1994. Recommendation for the characterisation of porous solids. *Pure and Applied Chemistry*, **66**, 1739–1758, https://doi.org/10.1351/pac199466081739

Rutqvist, J. 2012. The geomechanics of CO_2 storage in deep sedimentary formations. *Geotechnical and Geological Engineering*, **30**, 525–551, https://doi.org/10.1007/s10706-011-9491-0

Sheldon, H.A., Wheeler, J., Worden, R.H. and Cheadle, M.J. 2003. An analysis of the roles of stress, temperature, and pH in chemical compaction of sandstones. *Journal of Sedimentary Research*, **73**, 64–71, https://doi.org/10.1306/070802730064

Slatt, R.M. and O'Brien, N.R. 2011. Pore types in the Barnett and Woodford gas shales: contribution to understanding gas storage and migration pathways in fine-grained rocks. *American Association of Petroleum Geologist Bulletin*, **95**, 2017–2030, https://doi.org/10.1306/03301110145

Sorkhabi, R. 2014. Fracture, fracture everywhere Part I. *GeoEXPRO*, **11**, 86–90.

Span, R. and Wagner, W. 1996. A new equation of state for carbon dioxide covering the fluid region from the triple-point temperature to 1100 K at pressures up to 800 MPa. *Journal of Physical and Chemical Reference Data*, **25**, 1509–1596, https://doi.org/10.1063/1.555991

Spencer, C. 1987. Hydrocarbon generation as a mechanism for overpressuring in Rocky Mountain Region. *American Association of Petroleum Geologists Bulletin*, **71**, 368–388.

Springer, N. and Lindgren, H. 2006. Caprock properties of the Nordland Shale recovered from the 15/9-A11 well, the Sleipner area. *Greenhouse Gas Technology Conference 2006 (GHGT-8) Proceedings*, 1–6, 19–22 June. Trondheim, Norway.

Stork, A.L., Verdon, J.P. and Kendall, J.M. 2015. The microseismic response at the in Salah Carbon Capture and Storage (CCS) site. *International Journal of Greenhouse Gas Control*, **32**, 159–171, https://doi.org/10.1016/j.ijggc.2014.11.014

Swarbrick, R.E. and Lahann, R.W. 2016. Estimating pore fluid pressure-stress coupling. *Marine and Petroleum Geology*, **78**, 562–574, https://doi.org/10.1016/j.marpetgeo.2016.10.010

Tiab, D. and Donaldson, E.C. 2016*a*. Introduction to petroleum geology. *Petrophysics*. 4th edn. Elsevier, 23–66, https://doi.org/10.1016/B978-0-12-803188-9.00002-4

Tiab, D. and Donaldson, E.C. 2016*b*. Naturally fractured reservoirs. *Petrophysics*. 4th edn. Elsevier, 415–481, https://doi.org/10.1016/B978-0-12-803188-9.00008-5

Tissot, B., Durand, B., Espitalie, J. and Combaz, A. 1974. Influence of nature and diagenesis of organic matter in formation of petroleum. *American Association of Petroleum Geologist Bulletin*, **58**, 499–506.

Tonnet, N., Mouronval, G., Chiquet, P. and Broseta, D. 2011. Petrophysical assessment of a carbonate-rich caprock for CO_2 geological storage purposes. *Energy Procedia*, **4**, 5422–5429, https://doi.org/10.1016/j.egypro.2011.02.527

Udo, K.I., George, N.J., Akankpo, A.O., Azuoko, G.B. and Aka, M.U. 2020 Determining fracture pressure gradients from well logs. *International Journal of Advanced Geosciences*, **8**, https://doi.org/10.14419/ijag.v8i1.29162

Velázquez-Cruz, D., Espinosa-Castañeda, G., Díaz-Viera, M.A. and Leyte-Guerrero, F. 2017. Determination of pore pressure using divergences. *International Journal of Petroleum Science and Technology*, **11**, 51–63.

Venaruzzo, J.L., Volzone, C., Rueda, M.L. and Ortiga, J. 2002. Modified bentonitic clay minerals as adsorbents of CO, CO_2 and SO_2 gases. *Microporous and Mesoporous Material*, **56**, 73–80, https://doi.org/10.1016/S1387-1811(02)00443-2

Wang, C. and Xie, X. 1998. Hydrofracturing and episodic fluid flow in shale-rich Basins_ A numerical study. *American Association of Petroleum Geologists Bulletin*, **82**, 1857–1869.

Wang, X., Jiang, Z., Jiang, S., Chang, J., Zhu, L., Li, X. and Li, J. 2019. Full-scale pore structure and fractal

Downloaded from https://www.lyellcollection.org by University of Liverpool on Jan 26, 2023

dimension of the Longmaxi Shale from the Southern Sichuan Basin: investigations using FE-SEM, gas adsorption and mercury intrusion porosimetry. *Minerals*, **9**, https://doi.org/10.3390/min9090543

Watts, N.L. 1987. Theoretical aspects of cap-rock and fault seals for single- and two-phase hydrocarbon columns. *Marine and Petroleum Geology*, **4**, 274–307, https://doi.org/10.1016/0264-8172(87)90008-0

Worden, R.H., Charpentier, D., Fischer, Q. and Aplin, A.C. 2005. Fabric development and the smectite to illite transition in Upper Cretaceous mudstones from the North Sea: an image analysis approach. *Geological Society, London, Special Publications*, **249**, 103–114, https://doi.org/10.1144/GSL.SP.2005.249.01.09

Worden, R.H., Allen, M.J. *et al*. 2020. Lower Cretaceous Rodby and Palaeocene Lista shales: characterisation and comparison of top-seal mudstones at two planned CCS Sites, Offshore UK. *Minerals*, **10**, https://doi.org/10.3390/min10080691

Xin, F., Xu, H., Tang, D., Yang, J., Chen, Y., Cao, L. and Qu, H. 2019. Pore structure evolution of low-rank coal in China. *International Journal of Coal Geology*, **205**, 126–139, https://doi.org/10.1016/j.coal.2019.02.013

Xinong, X., Sitian, L., Weiliang, D. and Qiming, Z. 1999. Overpressure development and hydrofracturing in the Yinggehai Basin, South China Sea. *Journal of Petroleum Geology*, **22**, 437–454, https://doi.org/10.1111/j.1747-5457.1999.tb00478.x

Yang, Y.L. and Aplin, A.C. 1998. Influence of lithology and compaction on the pore size distribution and modelled permeability of some mudstones from the Norwegian margin. *Marine and Petroleum Geology*, **15**, 163–175, https://doi.org/10.1016/s0264-8172(98)00008-7

Yang, Y. and Aplin, A.C. 2007. Permeability and petrophysical properties of 30 natural mudstones. *Journal of Geophysical Research*, **112**, https://doi.org/10.1029/2005jb004243

Yardley, G.S. and Swarbrick, R. 2000. Lateral transfer: a source of additional overpressure? *Marine and Petroleum Geology*, **17**, 523–537, https://doi.org/10.1016/S0264-8172(00)00007-6

Yven, B., Sammartino, S., Geraud, Y., Homand, F. and Villieras, F. 2007. Mineralogy, texture and porosity of Callovo-Oxfordian argillites of the Meuse/Haute-Marne region (eastern Paris Basin). *Mémoires de la Société géologique de France*, **178**, 73–90.

Zhang, J., Liu, G., Torsaeter, O., Tao, S., Jiang, M., Li, G. and Zhang, S. 2020. Pore-throat structure characteristics and its effect on flow behavior in Gaotaizi tight siltstone reservoir, northern Songliao Basin. *Marine and Petroleum Geology*, **122**, https://doi.org/10.1016/j.marpetgeo.2020.104651

Zhang, N., Zhao, F., Guo, P., Li, J., Gong, W., Guo, Z. and Sun, X. 2018. Nanoscale pore structure characterization and permeability of mudrocks and fine-grained sandstones in coal reservoirs by scanning electron microscopy, mercury intrusion porosimetry, and low-field nuclear magnetic resonance. *Geofluids*, **2018**, 1–20, https://doi.org/10.1155/2018/2905141

Zhang, R. and Wu, Y. 2019. Hydrologic, mechanical, thermal, and chemical process coupling triggered by the injection of CO_2. *In*: Newell, P. and Ilgen, A.G (eds) *Science of Carbon Storage in Deep Saline Formations*. Elsevier, 361–381.

Zoback, M.D. 2007. *Reservoir Geomechanics*. Cambridge University Press, Cambridge.